Grain boundary phases in bcc metals

Grain boundary phases in bcc metals

T. Frolov,[1] W. Setyawan,[2] R. J. Kurtz,[2] J. Marian,[3] A. R. Oganov,[4, *] R. E. Rudd,[1] and Q. Zhu[5]

[1]*Lawrence Livermore National Laboratory, Livermore, California 94550, USA*

[2]*Pacific Northwest National Laboratory,*

P. O. Box 999, Richland, Washington 99352, USA

[3]*Department of Materials Science and Engineering,*

University of California Los Angeles,

Los Angeles, California 90095, USA

[4]*Stony Brook University, Stony Brook, New York 11794, USA*

[5]*Department of Physics and Astronomy,*

High Pressure Science and Engineering Center,

University of Nevada, Las Vegas, Nevada 89154, USA

Abstract

We report a computational discovery of novel grain boundary structures and multiple grain boundary phases in elemental body-centered cubic (bcc) metals represented by tungsten, tantalum and molybdenum. While grain boundary structures created by the γ-surface method as a union of two perfect half crystals have been studied extensively, it is known that the method has limitations and does not always predict the correct ground states. Here, we use a newly developed computational tool, based on evolutionary algorithms, to perform a grand-canonical search of a high-angle symmetric tilt and twist boundaries in tungsten, and we find new ground states and multiple phases that cannot be described using the conventional structural unit model. We use molecular dynamics (MD) simulations to demonstrate that the new structures can coexist at finite temperature in a closed system, confirming these are examples of different grain boundary phases. The new ground state is confirmed by first-principles calculations.

I. INTRODUCTION

Grain boundaries (GBs) play a key role in the mechanical behavior of materials.[1] Their structure affects a diverse range of properties including fracture, recrystallization, and creep.[2–4] The abundance of GBs in nanocrystalline materials makes the boundaries particularly important in the class of advanced materials being developed for their promise of radiation tolerance and the combination of ductility with strength.[5]

Growing number of experimental and modeling studies suggest that behavior of GBs at the nanoscale can be richer than previously thought.[6] Abrupt transitions in properties of bicrystals[7,8] and polycrystalline materials[9–11] suggest that similar to bulk materials GBs can exist in different phases and exhibit first-order phase transitions. In doped ceramic and metallic systems transitions between clean, monolayer, bilayer, trilayer, and nanoscale intergranular films of different thickness have been proposed to play crucial role in abnormal grain growth[10], solid-state activated sintering[12] and liquid metal embrittlement.[3] These experimental studies demonstrated orders of magnitude changes in GB reduced mobility upon doping and suggested new opportunities for design of microstructures at the nanoscale through kinetic GB engineering.[10]

Much of the existing evidence for first-order transitions at GBs is indirect. While the experimental observation of GB structure at the nanoscale is often challenging,[13–16] modeling has provided important new insights into GB phase transitions. Recently, improved simulation methodology demonstrated new ground states and first-order GB transitions in several face-centered cubic (fcc) metals including Cu, Ag, Au and Ni.[17,18] These studies systematically explored GB energetics as a function of the number of atoms at the boundary. MD simulations demonstrated fully reversible first-order transitions between grain boundary phases with different atomic densities triggered by temperature, changes in chemical composition and concentration of point defects.[17–20] While GBs in bcc metals have also been investigated by atomistic simulations extensively,[21–26] little is know about their phase behavior and possibility of first order transitions apart from the recently found dislocation pairing transition in low-angle iron GBs composed of discrete dislocations.[27]

In this work we use a new computational tool[18] to investigate the structure of GBs in the bcc metal tungsten. The choice of this material system is motivated by the use of tungsten for magnetic fusion energy applications. The ultimate success of fusion technology depends on materials that can survive the harsh operating environment. Tungsten has been selected as the divertor material in the International Thermonuclear Experimental Reactor (ITER)[28] and is a leading candidate for additional plasma-facing components in the planned follow-on tokamak DEMO[29] because of its high mechanical strength, high thermal conductivity, high melting

point and low yield for sputtering. While tungsten has a number of favorable properties, it is also intrinsically brittle even at relatively high temperatures especially after recrystallization.[30] Accurate prediction of grain boundary structure and possible transitions are important for strategies that aim to improve the ductility of tungsten by alloying and understanding how radiation damage is absorbed by grain boundaries at the nanoscale. In this work, we find new ground states and demonstrate phase transitions in high-angle tilt and twist GBs in tungsten and show the role of these transitions in the absorption of point defects.

II. METHODOLOGY

A. Model system

For our study we selected the $\Sigma27(552)[1\bar{1}0]$ symmetric tilt and two $\Sigma5(001)$ twist GBs as representative high-angle high-energy boundaries. The symmetric tilt boundary was obtained by a $148°$ degree rotations of two grains around a common $[1\bar{1}0]$ tilt axis. The two twist boundaries were obtained by $36.87°$ and $53.13°$ rotation of the grains around a common $[001]$ axis with the GB plane perpendicular to the axis of rotation. Based on the indexes of the bulk crystals we refer to the $36.87°$ boundary as (310)-twist, and the $53.13°$ boundary as (210)-twist. We modeled the GBs in tungsten using two interatomic potentials, EAM1[31] and EAM2[32], as well as density functional theory (DFT) calculations.[33,34] The $\Sigma5$ twist boundaries are popular model systems that have been investigated in a variety of materials including tungsten.[35–37] The choice of the symmetric tilt boundary was motivated by several recent DFT studies that investigated $[1\bar{1}0]$ symmetric tilt boundaries to screen for alloying elements that would improve ductility of tungsten.[38–41] Small amounts of added elements may have a dramatic effect on the fracture toughness of a material.[3,30,42,43] These DFT simulations evaluate the propensity of the system to undergo GB fracture by calculating the cleavage energy, which is the difference $\gamma_{GB} - 2\gamma_{FS}$ between the boundary energy and the energy of the two free surfaces.[44] The calculations showed that segregation to different boundary sites may have opposing effects on the cleavage energy: segregation to some sites improves GB cohesion, while segregation to other sites promotes embrittlement.[38] The energy of segregation to different GB sites strongly depends on the local atomic environment, i. e., the boundary structure.[33,39,45] Thus, a correct prediction of GB structure is necessary for the accuracy of such strategies.

B.   GB structure generation

1.   *γ-surface method*

First, we constructed the GBs using the γ-surface method, which was also employed in previous studies of this boundary.[34,39–41] In this approach two misoriented perfect half-crystals are joined together while sampling different translations of the grains parallel to the GB plane. The lowest energy GB configurations are assumed to be the ground state in these calculations. During the minimization, no atoms are added or removed from the GB core. In addition, the configurational space of possible GB structures explored during the energy minimization is rather limited.

A number of computational studies in several different materials systems demonstrated limitations of this approach and suggested that a more thorough sampling that includes the optimization of the number of atoms at the grain boundary is needed. For example, in ionic materials low-energy grain boundary structures were found when a certain fraction of ions was removed from the GB core prior to the energy minimization.[37,46,47] Simulated quenching to the zero-temperature limit of the grand-canonical ensemble demonstrated low-energy GB structures of a high-angle twist grain boundary in fcc Cu with different numbers of atoms.[48] An investigation of Si twist boundaries revealed the importance of sampling and optimization of the atomic density and contrary to prior calculations demonstrated distinctly ordered ground states at 0 K.[35] Genetic algorithms designed to explore a diverse population of possible structures were applied to search for low-energy structures in symmetric tilt Si grain boundaries[49] and multicomponent ceramic grain boundaries.[50]

Recent modeling in fcc metals showed that structure of relatively simple [001] symmetric tilt boundaries GBs can be surprisingly complex and have multiple phases.[8,17,18] The new structures were found to have different atomic densities and complex atomic ordering with the periodic unit many times larger than that of the bulk crystals. Beyond symmetric tilt boundaries, continuous vacancy loading into general grain boundaries in Cu revealed lower energy states with different atomic density.[51] In bcc metals, recent computational studies demonstrated that changing the number of atoms in the GB core increases[52] and in some boundaries decreases GB energy.[36,53]

2. Grand-Canonical Evolutionary Search

Despite its limitations, the γ-surface approach remains the most commonly used method to construct GBs at 0 K, largely because no other robust computational tool of GB structure prediction is available. On the other hand, much progress has been made in developing of computational tools to predict structures of crystals.[54] One such method is USPEX[55], which uses evolutionary algorithms to predict the structure of materials based on the compositions alone. USPEX has proved to be extremely powerful in different systems including bulk crystals[55], 2D crystals[56], surfaces[57], polymers[58] and clusters.[59] In this work we use a recently developed computational tool[18] based on the USPEX code[55,59,60] to explore structures and possible phase behavior of the $\Sigma27(552)[1\bar{1}0]$ symmetric tilt and the $\Sigma5(001)$ twist GBs. In this approach a population of 50 to 100 different GB structures evolves over up to 50 generations by operations of heredity and mutation to predict low-energy configurations. The mutation operations include the displacements of atoms, insertion and removal of atoms from the GB core and sampling of larger-area GB reconstructions.[18]

In our method, we split the bicrystal into three different regions, the upper grain (UG), the lower grain (LG), and the grain boundary (GB). UG and LG regions are taken to be 40 Å thick. The GB thickness is an input parameter defined by the user. To ensure accurate GB energy calculation converged with respect to the system size normal to the grain boundary plane, we sandwich the GB region between two 20 Å thick buffer regions. The atoms in the buffer zones are not affected by the evolutionary search, but can move freely during the energy minimization. We create the first generation of GB structures by randomly populating GB regions with atoms, imposing layer group symmetries[59] selected at random for each bicrystal, and then joining the three regions together applying random relative translations parallel to the grain boundary plane. The enforced symmetry is used to avoid liquid-like structures with close energies that are likely to produce similar children with poor fitness. This initial symmetry can be broken or lowered by the subsequent variation operations like heredity and mutation. The number of atoms placed in each GB slab is estimated initially from the bulk density of the perfect crystal and the thickness defined by the user. This number is then randomly varied within the interval from 0 to $N_{\text{plane}}^{\text{bulk}}$, where $N_{\text{plane}}^{\text{bulk}}$ is the number of atoms in one bulk atomic plane parallel to the GB. This ensures that structures with different atomic densities are present in the initial population. The atomic fraction [n] for each grain boundary structure is calculated according to $[n] = (N \text{ modulo } N_{\text{plane}}^{\text{bulk}})/N_{\text{plane}}^{\text{bulk}}$, where N is the total number of atoms in the GB region. We also implemented constrained searches where [n] of all GB structures in the population is within a certain interval. In the population the different bicrystals have different GB dimensions

5

generated as random multiples of the smallest periodic GB unit.[61] The structures generated by the algorithm are relaxed externally by the LAMMPS code[62] and the grain boundary energy is determined and serves as a fitness parameter. During the optimization, the atoms in the GB region need to be fully relaxed, while the atoms in the bulk only move as rigid bodies.

Each successive generation is produced by operations of heredity and mutations, by selecting the structures with the lowest 60% of the energies as parents. In the heredity operation two grain boundary structures are randomly sliced and the parts from different parents are combined to generate the offspring. In a mutation operation the grain boundary atoms are displaced according to the stochastically picked soft vibrational modes based a bond-hardness model.[59,61] Such mutations are advantageous to purely random displacements because they mimic a structural transition due to phonon instability upon large elastic strains and are more likely to lead to children structures with low-energy. To sample different atomic densities atoms in the grain boundary region are inserted and deleted.[18,59] The atoms are removed based on the value of the local order parameter calculated for each atom. The order parameter is described in Eq. (5) of Ref.[63]. To insert atoms into the GB slab, we identify the empty sites by constructing a uniform grid with a resolution of 1 Å^3 and fill them at random. To ensure relatively gradual changes in the GB structure, the random number of the inserted and removed atoms also does not exceed 25% of the total number of atoms in the GB slab. A more detailed description of the algorithm can be found in Ref.[18].

3.   *DFT calculations*

Energies of thirteen best GB structures of the $\Sigma27(552)[1\bar{1}0]$ symmetric tilt GB generated using the empirical potentials were refined with DFT calculations. The calculations were performed with VASP software version VASP.5.4.1.[64,65] Projector-augmented-wave (PAW)[65] pseudopotential for W was taken from the PAW datasets v.52 where electrons in the 5d and 6s orbitals were treated as valence. Perdew-Burke-Ernzerhof (PBE)[66] functionals were employed for the electronic exchange-correlation energies. To reduce the computational cost of the DFT calculations the number of atoms in the simulation cells was reduced by removing some part of the bulk atoms. The simulation blocks contained either 276 or 278 atoms depending on the GB structure. The z dimension was set to 50 Å, leaving at least 20 Å of vacuum to avoid surface-surface interactions. We also performed energy calculations for simulation blocks without GBs containing slabs with two {552} surfaces. The xy dimensions was a 2×2 supercell of the {552} surface unit cell and contained 4 atoms per {552} layer. For brevity, SLAB M refers to a slab

with M atoms without a GB. SLAB276 and SLAB280 were created.

All structures were relaxed until the total energy converged to within 10 meV. In both the GB and the slab systems, the size of the simulation cells was fixed to ensure the identical lattice parameters in the bulk. The lattice parameter was set to be equal to the lattice constant of a fully relaxed block with all periodic boundary conditions. GB energy was then calculated as the difference between the energies of the slabs with and without GBs corrected for the difference in the number of atoms

$$E_{\mathrm{GB}} = \frac{1}{A} \left[E\{GB\} - E\{SLAB276\} - (E\{SLAB280\} - E\{SLAB276\}) \frac{N - 276}{4} \right] \quad (1)$$

where A is the GB area, $E\{GB\}$ is the total energy of the GB slab containing N atoms.

Convergence with respect to plane-wave energy cutoff (ENCUT) and the number of **k**-points was studied using the system with 276 atoms the grain boundary labeled as GB14 in Table II . Γ-centered **k**-point grid was employed.

III. RESULTS

A. GB structures at zero temperature

1. $\Sigma 27(552)[1\bar{1}0]$ symmetric tilt GB

Fig. 1 illustrates the lowest energy γ-surface configurations of the GB predicted by DFT calculations in Ref.[67] (Fig. 1a) and the current work using the two interatomic potentials (Fig. 1b). The structural units of both configurations are outlined with an orange curve to guide the eye. Notice that within the γ-surface approach, DFT and the empirical potentials predict somewhat different structures. This result is consistent with previous studies that identified multiple metastable and energy-degenerate states generated by this methodology.[53] The view of the boundary structure along the tilt axis shown in the right-hand panel of Fig. 1 demonstrates that in both structures the atoms are confined to misoriented (110) planes of the two crystals. By construction, these GB structures can be mapped atom by atom onto a displacement symmetry conserving (DSC) lattice,[1] which is the coarsest lattice that contains all of the atoms of both misoriented crystals on its lattice sites.

Fig. 2 a and b illustrate the results of the evolutionary searches performed using the EAM1 and EAM2 potentials, respectively. Each blue circle on the plot corresponds to a grain boundary structure generated during the search. The grain boundary energy is plotted as a function of the

number of atoms [n] expressed as a fraction of atoms in the bulk (552) plane. The red diamonds on the plots represent the best configurations generated by the γ-surface approach. At [n]=1/2 the search with both potentials predicted new ground states of this boundary with energies 7-12% (depending on the potential) lower than that of the γ-surface generated structures. Fig. 3 illustrates the structures of several [n]=1/2 GBs predicted by the two potentials. To obtain these ground states, a number of atoms equal to half (1/2) of the (552) atomic plane must be inserted into the GB core. This explains why these structures have not been discovered by the γ-surface method. The low-energy states represent 2×2 and 2×3 unit cell reconstructions and cannot be found in a standard 1×1 unit cell. At [n]=0 the EAM2 potential[32] also predicts a different low-energy GB structure, labeled as GB12, that does not require addition or removal of atoms. The boundary structure is illustrated in Fig. 4. The energy of this structure is nearly the same energy as the new ground state at the $[n] = 1/2$ atomic fraction and represents what may be a different phase of this boundary. The search with EAM2 potential clearly demonstrates that insertion or removal of atoms is not the only shortcoming of the γ-surface method: even at [n]=0 there may be distinct local minima, so prediction of grain boundary structure requires advanced sampling of many possible configurations.

To extend the predictions of the new ground state and possible multiple phases of the $\Sigma 27 (552)[1\bar{1}0]$ GB to other bcc metals, we performed evolutionary GB structure searches for the same symmetric tilt GB in Ta and Mo. Ta was modeled with an angular-dependent EAM potential (ADP),[68] while Mo was modeled with a EAM potential.[69] The results of the search for the two metals are illustrated in Fig. 5. The Ta search predicts three distinct low-energy configurations at [n]=0, [n]=1/3 and [n]=1/2. These three structures are illustrated in Fig. 6a, b and c, respectively. The [n]=0 and [n]=1/2 Ta structures match the GBs with the same atomic densities generated using the EAM2 potentials in W. The [n]=0 structures match exactly, while the [n]=1/2 minimum in Ta is a larger 2×3 GB area reconstruction. The ground state structure at [n]=1/3 shown in Fig. 6b closely resembles the [n]=0 state. However, it has a higher atomic density and is also a larger 2×3 reconstruction than the [n]=0 state in the same material.

The results of the Mo search showed one strong minimum at [n]=2/3. The ground state GB structure is illustrated in Fig. 5d and represent a denser variation of the ground state [n]=1/2 phase found in W, it is also a larger 2×3 reconstruction. Thus, the evolutionary searches in Ta and Mo found grain boundary phases similar to the structures identified in W. In different bcc metals these similar structures of the $\Sigma 27 (552)[1\bar{1}0]$ GB have slightly different atomic densities and areas.

2. $\Sigma5(001)$ twist GBs

Fig. 7 a and b illustrate the results of the evolutionary searches for the $\Sigma5(001)$ (210)-twist and $\Sigma5(001)$ (310)-twist GBs performed using EAM2 potential for tungsten. Fig. S1. shows the results of the evolutionary search performed for the two boundaries in Mo and Ta. In all models both boundaries have the ground state structures at 0K with the atomic density of [n]=1/5. The energies of these ground states are significantly lower than the energies of the best configurations at [n]=0, which again points to the limitations of the γ-surface approach and emphasizes the importance of the grand-canonical search.

In addition to the ground state at [n]=1/5, the evolutionary searches found competing low-energy structures at [n]=2/5 for both twist boundaries. Fig. S2. shows the lowest energy structures at [n]=1/5 and [n]=2/5 of the $\Sigma5(001)$ (210)-twist boundary predicted by the evolutionary search in W, Mo and Ta. Fig. 8 shows (a) the [n]=1/5 ground state as well as (b) and (c) two variants of the [n]=2/5 GB structures of the $\Sigma5(001)$ (310)-twist boundary in tungsten. The two variants of the [n]=2/5 structure appear similar in the left-hand side panels, but have different structures when viewed in the middle panels. The variance shown in Fig. 8c has the lowest energy at [n]=2/5, while the energy of the other structure shown in Fig. 8b is 0.9% higher. With the only exception of the Mo model, which did not predict a low-energy state of the $\Sigma5(001)$ (310)-twist boundary near [n]=2/5, the results of the evolutionary search are very consistent for both boundaries in the three metals studied.

3. DFT calculations for the $\Sigma27(552)[1\bar{1}0]$ symmetric tilt boundary

To refine the energies of the new GB structures predicted in this work with DFT calculations we selected the $\Sigma27(552)[1\bar{1}0]$ GB in W. The new ground states of this GB predicted by the evolutionary search are not unique. The searches with the two potentials identified about thirty distinct low-energy configurations all within a 2% energy range (approximately 0.05 J/m^2). The energies of the best thirteen configurations were subsequently refined with DFT calculations. Table I shows the results in which ENCUT = 250 eV and $2\times4\times1$ **k**-point grid was sufficient to converge the grain boundary energy to within 10 mJ/m^2. Therefore, the rest of the calculations were performed with this setting. The results of the GB energy calculations are summarized in Table II. The DFT calculations confirmed that [n]=1/2 ground states predicted by both potentials have essentially the same energy. Fig. 3 illustrates four examples of the ground state structures. These boundaries correspond to GBs 11, 1, 2 and 3 in Table II. The structure in Fig. 3a was predicted by potential EAM2, while the other structures were generated using the the EAM1

potential. Each GB structure is shown from three different viewpoints. The left-hand side panel shows that all the structures are nearly indistinguishable when viewed projected on the plane normal to the $[1\bar{1}0]$ tilt axis, the standard view to visualize structural units. On the other hand, the middle and the right-hand panels show significantly different atomic arrangements. In the middle panels the tilt axis is parallel to the plane of the image, while the right-hand side panels show the structure within the GB plane viewed from the top. The top view in the right-hand side panels most clearly shows the difference between these ordered structures. In all of these configurations the atoms occupy sites between the $(1\bar{1}0)$ planes within the GB plane. These calculations show that a number of similar structures with the same GB energy can be generated by permuting the occupancy of atoms in different *interstitial* positions within the boundary. These structures can no longer be mapped onto a DSC lattice, and to distinguish them from the structures generated by the γ-surface approach we refer to them as non-DSC structures. This characteristic feature is remarkably similar to split-kite phases recently found in [100] symmetric tilt boundaries in Cu[17,18], suggesting that these non-DSC structures may be a general phenomenon.

At [n]=0 the predictions of the three models are less consistent. The DFT energies of the γ-surface structures GB10 (2.960 J/m^2) and GB13 (2.973 J/m^2) generated with the empirical potentials do not agree with the energy of the γ-surface structure GB14 (2.688 J/m^2) based only on DFT. The GB12 ground state at [n]=0 predicted by the evolutionary search with EAM2 potential was also not confirmed as a low energy state by the subsequent DFT calculations. It is possible that the evolutionary search that uses DFT calculations only would generate yet a different low-energy state at [n]=0. Unfortunately, such a calculation would be significantly more expensive. Nevertheless, within the DFT model the structures GB14 at [n]=0 with energy $\gamma_{\text{GB14}} = 2.68$ J/m^2 and GB1 at [n]=1/2 with energy $\gamma_{\text{GB1}} = 2.592$ J/m^2 represent two candidates for distinct grain boundary phases. The close energies at 0 K suggest the possibility of transitions between the two GB structures due to temperature, pressure or alloying.

B. High-temperature MD simulations

The large number of GB configurations nearly degenerate in energy found by the evolutionary search at 0 K suggests new questions about the structures of these grain boundaries at finite temperature. Can some of the different grain boundary structures coexist in equilibrium? How does the multiplicity of similar [n]=1/2 structures of the symmetric tilt boundary affect the finite-temperature structure? Which variant of the [n]=2/5 structure of the (310)-twist boundary

is stable at finite temperature? The abundance of similar structures may contribute to the configurational entropy of the boundary at finite temperature[36], since many different states can be created by permutations of atoms in different sites within the boundary with a negligible penalty in energy.

1. $\Sigma 27(552)[1\bar{1}0]$ symmetric tilt GB in W

To investigate the effect of temperature on [n]=1/2 structure of the $\Sigma 27(552)[1\bar{1}0]$ GB in W, we performed a molecular dynamics simulation for 100 ns at high temperature (2500 K) with the EAM1 potential. To avoid bias toward one of the newly identified [n]=1/2 ground states, we used a higher-energy structure predicted by the γ-surface approach (Fig. 1b) as the initial configuration. Along the x direction we terminated the GB with two $(\bar{1}15)$ surfaces to allow atoms to diffuse in and out, enabling the atomic density in the GB core to vary.[17] During the simulation, the GB transforms to its non-DSC state. The equilibrium high-temperature structure is illustrated in Fig. 9. The simulation confirms that the non-DSC ground state identified by the evolutionary search remains the minimum free energy structure at high temperature. Fig. 9c shows the structure of the boundary when viewed from the top. This number of atoms [n] is a function of temperature, pressure and chemical potential which is set by the open surface in this case. Throughout the manuscript we refer to the different GB phases by their values of [n] at 0 K for convenience. At this temperature and system size we calculated the number of atoms to be approximately [n]=0.59. As expected, it deviates from its 0 K value of 1/2, but it is reasonably close and consistent with presence of other similar higher energy, higher density states generated by our evolutionary search. Calculating [n] for a high-temperature GB structure is not always straightforward. Atomic vibrations, closely spaced high index planes, elastic distortions due to surfaces and other GB structures as well as rigid shifts of the bulk grains relative to each other may make it difficult to extract a rectangular periodic region containing the boundary and the bulk necessary for calculations of [n]. To address this challenge with relax the atomic structure to get rid of the vibrations and carve out a portion of the block with the upper and the lower bulk planes parallel to the GB. Along the x direction we follow the low-index [100] planes in each crystal, so the carving planes are V-shaped on each side. The positions of the V-shaped planes are chosen to select multiples of periodic GB unit in the x direction. Since the simulation block was periodic in the y-direction, there was no need to construct cutting planes. The portion of the block that was carved out for calculating [n] was selected sufficiently far enough from surfaces and we varied the x dimension of the region from 1.64 nm to 8.02 nm to make sure that [n] is

not sensitive to the choice of location of the region within the boundary.

The high-temperature pattern shown in Fig. 9 formed by the GB atoms which are colored in orange does not match exactly any of the states generated at 0 K, shown in Figs. 3. Rather, it can be described as a mixture[36,70] of different [n]=1/2 and other [n] patterns generated in the smaller periodic cells at 0 K. The image in Fig. 9c also suggests that the periodicity of atomic columns shown in orange appears to be incompatible with the bulk periodicity along the [110] direction and no clear periodic GB unit smaller than the periodic unit of the simulation block can be identified in this high-temperature simulation. It is possible that the high-temperature structure can be aperiodic. These observations suggest that the estimation of the configurational entropy of this GB due to the multiplicity of similar states based on structures generated at 0 K alone may not be straightforward.

The left surface of the bicrystal shows a *chevron* reconstruction[71,72]. Near the chevron the first two GB units have a different structure closely resembling the [n]=0 non-DSC ground state GB12 identified using the other (EAM2) potential. This example also shows that the GB structure in a polycrystalline metal will be influenced by local mechanical forces (e.g. triple junctions, GB defects, nearby lattice dislocations, etc.)

The evolutionary search with the EAM2 potential predicts two distinct low-energy structures with [n]=0 and [n]=1/2. MD simulations of the individual structures at T=2000 K and T=2500 K with periodic boundary conditions confirmed that both are stable at finite temperature. To test whether the two types of structures can coexist we created a simulation block with dimensions $49.5 \times 2.7 \times 13.0$ nm^3 and periodic boundary conditions along the boundary. The initial GB structure was set to GB12 and had 159120. Then, additional 153 atoms were inserted at random positions in one half of the bicrystal at a distance 5 to 10 Å above the GB plane. This configuration was annealed at 2000 K for 200 ns. During the first few nanoseconds of the simulation the added atoms diffused into the GB and about half of the total GB area transformed into the [n]=1/2 structure. After that, the two grain boundary structures continued to coexist for the rest of the simulation and we observed no further transformations. Fig. 10 illustrates the [n]=0 and [n]=1/2 grain boundary phases coexisting in equilibrium. The two structures are separated by a line defect that spans the periodic length of the simulation block. The position of this line defect fluctuates during the simulation.

The equilibrium heterogeneous state of the boundary obtained in the MD simulations is consistent with GB energetics explored with the evolutionary search at 0 K. According to the 0 K analysis, GB structures with densities between [n]=0 and [n]=1/2 have high energies, which means that the boundary with such density can lower its free energy by phase separating. The

lower free energy state is composed of two homogeneous GB phases with their area fractions determined by the lever rule. In our MD simulations, introducing extra atoms to one of the GB phases effectively forced the system to enter the miscibility gap and phase separate. In simulation blocks with a planar GB phase junction, the subsequent addition of atoms does not change the state of the system but simply varies the area fraction of each GB phase. The concentration of atoms or point defects in each of the GB phases at a fixed pressure in the bulk is determined by the GB phase equilibrium (which sets the chemical potential value) and the temperature. This concentration is expected to deviate from 0 K values as well as the number of atoms in the same GB connected to open surfaces. Using the methodology described above we calculated $[n] \approx 0.77$ for the denser GB phase and $[n] \approx 0$ for the other structure. The latter number closely matches the 0 K value, even though we observe GB diffusion.

The coexistence simulation demonstrate that the two types of structures predicted by the evolutionary search represent two GB phases. The transformation is first-order and results in a discontinuous change in excess GB properties. This is to be contrasted to higher order transitions such as continuous premelting when only one GB state can exist at given temperature and pressure. To the best of our knowledge this is a first demonstration of phase behavior of high-angle GBs in a bcc material.

2. $\Sigma 5(001)$ *(310)-twist GB in W*

The evolutionary search at 0 K predicted two competing GB structures for both $\Sigma 5(001)$ twist boundaries studied in this work. To investigate GB phase transitions and co-existence at finite temperature we selected the $\Sigma 5(001)$ (310)-twist boundary. The [n]=1/5 ground state and two variants of the [n]=2/5 were first simulated separately using simulation blocks with periodic boundary conditions applied along the GB plane. The isothermal simulations were performed at 2000 K, 2500 K and 3000 K. The [n]=1/5 remained stable at all studied temperatures. On the other hand, the lowest energy [n]=2/5 variant shown in Fig. 8 c transforms into the variant shown in Fig. 8 b. During this transformation the number of atoms at the GB does not change. Thus, for [n]=2/5 constrained number of atoms in the system the GB structure shown in Fig. 8 b is a more stable variant at the simulated high temperatures.

To demonstrate a GB phase transition and coexistence in this twist boundary, we created a large simulations block with dimensions $20 \times 6.5 \times 6.5$ nm^3 which contained 41040 atoms. The [n]=1/5 ground state structure was selected as the initial configuration. We then introduced 120 interstitial atoms above the GB plane. During the subsequent anneal we observed nucleation

and growth of the [n]=2/5 GB phase. After the transformation the two GB structures coexisted in equilibrium while exchanging atoms by GB diffusion. In this block geometry, the grain boundary phase junctions, i. e. the line defects separating the different GB phases, span the periodic length of the simulation block in the y direction. This coexistence simulation in the (310)-twist boundary is analogous to the GB phase coexistence simulation in the symmetric tilt boundary.

To simulate a new GB phase nucleation event at the (310)-twist boundary, we created a different simulation block with dimensions $20 \times 24.5 \times 6.5$ nm^3 and 164160 atoms by replicating the previous defect free block four times along the y direction. In this block the GB had approximately square dimensions. Then we introduced 480 interstitial atoms inside a $10 \times 10 \times 0.5$ nm^3 bulk region above the GB plane and annealed the system for several tens of nanoseconds at 2000 K, 2500 K and 3000 K in three different simulations. During the anneal we observed a nucleation of the [n]=2/5 GB phase. Fig. 11a illustrates the heterogeneous structure of the boundary plane after the system was annealed at 3000 K for 200 ns. The nanoscale nucleus of the [n]=2/5 GB phase is located in the middle of the GB plane. It is embedded in the parent [n]=1/5 GB phase. The diameter of the nucleus in this simulation is around 7 nm. Its size is determined by the number of injected atoms as well as the temperature. The atoms in Fig. 11a are colored according to the coordination analysis as implemented in OVITO visualization tool.[73] The structure of the boundary in Fig. 11a was visualized by taking a cut parallel to the GB plane. The two GB structures have different hight along the z direction, which made the two GB phases appear in different colors along the cut. Fig. 11b illustrates another cut that goes through the nucleus parallel to the xz plane. This cut clearly demonstrated that the nucleus located in the middle is composed of the [n]=2/5 phase and is surrounded by the parent [n]=1/5 GB phase. The cut also reveals that the two GB phases have different z-positions, meaning that they form two steps. This is similar to the two GB phase structure modeled in the $\Sigma 27(552)[1\bar{1}0]$ symmetric tilt boundary. Fig. 11c and d show the zoomed in views of the two GB phases. The shape of the nucleus is not spherical, with the GB junction forming long straight segments. This shape is likely to be influenced by both the elastic interactions as well as the energetic anisotropy of the GB phase junctions.

IV. DISCUSSION AND CONCLUSIONS

In conclusion, using the evolutionary grand-canonical search we find new ground states and multiple GB phases with different atomic densities [n] in high-angle high-energy symmetric tilt

and twist GBs in bcc metals. Common simulation methodologies such as the γ-surface method often predict relatively simple structures for symmetric tilt boundaries, which are composed of kite-shaped units such as illustrated in Fig. 1. Their structure can be described within the structural unit model which is based on bulk crystallography.[53] For this reason symmetric tilt boundaries are considered to be some of the simplest boundaries, and they are popular model systems. In this work we have demonstrated that in bcc material such as tungsten, the structure of symmetric tilt boundaries can be significantly more complex.

Our calculations with two interatomic potentials for tungsten and DFT predict a new ground state of the $\Sigma 27(552)[1\bar{1}0]$, which requires additional atoms equivalent to half of a (552) atomic plane. We found similar low-energy structures using empirical potentials for Ta and Mo. The lack of atomic density optimization and the absence of sufficient sampling are the two main reasons this ground state was not found previously. The new ground state structures are characterized by complex arrangement of atoms within the GB plane. The boundaries are composed of a number of atoms incompatible with the number of atoms per atomic plane in the abutting grains. The GB structure cannot be mapped onto the DSC lattice. The ground state is degenerate, represented by a large number of similar structures with the same energy. This configurational complexity has consequences for the finite-temperature GB structure, which can be described as a combination of states found at 0 K. The structural features are remarkably similar to split-kite phases found in symmetric tilt fcc GBs.[17,18]

Within the EAM2 model for tungsten the evolutionary search at 0 K identified two distinct low-energy GB structures with different atomic densities [n]=0 and [n]=1/2. These structures and their close variations ([n]=1/3) were also predicted in Ta using the ADP EAM model. The Mo searches with empirical potentials did not predict low-energy states at [n]=0 or [n]=1/3. While the GB structures in different bcc metals do not have to be identical, these results motivate further studies of these GB using evolutionary grand-canonical searches with more accurate potentials such as neural network potentials. Nevertheless, within the DFT model of tungsten the energy difference between the different structures GB14 and GB1 was only 3% suggesting that they are examples of two different GB phases. The closeness of the energies at 0 K indicates a possibility of first-order transitions between the two GB structures due to temperature, pressure or addition of solute atoms.

In the $\Sigma 5(001)$ (210) and (310)-twist boundaries in W, Ta and Mo studied in this work, at 0 K the evolutionary search finds a ground state at [n]=1/5 and a metastable state at [n]=2/5. The $\Sigma 5(001)$ (210)-twist boundary in W have been investigated recently[36] and also showed a decrease in energy with changing the number of atoms and an energy minimum at the same

fraction of [n]=1/5. Our search found another strong minimum at [n]=2/5 in both (210)-twist and (310)-twist boundaries. At 0 K the ground state and the metastable states have close energies but very different structures. In addition, we find two distinct variants of the metastable state in the (310)-twist GB characterized by somewhat different atomic arrangement and close energies.

Finding the metastable grain boundary structures at 0 K may be just as important as predicting the ground states. Temperature, pressure or chemical composition change the free energy of different GB states and can stabilize the metastable structures triggering GB phase transitions. The searches at 0 K provide valuable information about excess quantities of different GB structures and can be used to predict these transitions.[74] The free energy of each GB phase is a continuous function of the state variables as described by the Gibbs adsorption equation.[75] In the first-order transitions picture, the equation of state of each GB phase extends into the metastable region and transitions occur by nucleation. In addition two GB phases with the same free energy can coexist in equilibrium. Therefore, to demonstrate that the different GB structures found at 0 K are examples of GB phases we performed MD simulations of coexistence.

The coexistence simulations studied in this work are fundamentally different from phase equilibrium that can exist in fluid systems. Due to the presence of a lattice, changes in the number of atoms due to vacancies or interstitials provide solids with another thermodynamic degree of freedom. Thermodynamic descriptions that include these variations of state and describe their role in phase equilibrium were developed for bulk solids,[76–78] but not for interfaces. Similar to the bulk phases, the free energy of each GBs phase depends on the concentration of atoms (chemical potential) in addition to temperature, pressure and other state variables.[79,80] In the closed system coexistence simulations implemented in this work, the equilibrium between two different GB phases is established through exchange of atoms by means of GB diffusion. In these simulations, when one of the GB phases attempts to grow at the expense of the other phase by a fluctuation, interstitials or vacancies are produced because the two states have different atomic densities. Since these extra atoms or vacancies cannot escape to the surface, they are redistributed by diffusion among the two GB phases increasing the free energy of the growing phase. This increase stops further growth and eventually equilibrium concentration of atoms is established within each GB phase. In equilibrium both GB phases separated by the planar GB phase junction should have the same free energies and coexist in a range of temperatures. The solubility of atoms within each GB phase at coexistence is a function of temperature. This situation should be contrasted to GBs connected to sources of atoms such as surface steps, where at fixed hydrostatic pressure in the bulk two GB phases in an elemental system can coexist only

at one temperature. The coexistence simulations presented in this work motivate the general-ization of the thermodynamic treatment of GBs to include another degree of freedom due to the variation in the number of atoms in the adsorption equation. Such a theory would provide a framework necessary to quantify and describe the GB phase coexistence simulated in this study.

In the $\Sigma 5(001)$ (310)-twist boundary we also simulated stable coexistence between two GB phases separated by a non-planar GB phase junction. The obtained equilibrium nucleus represents a critical nucleus for a given value of chemical potential.[76–78] If the parent phase was infinitely large this nucleus would eventually dissolve. In our simulation it is stabilized due to finite size effects. Specifically, the size of the nucleus is comparable to the size of the parent GB phase. Similar modeling approaches have been demonstrated to stabilize critical nuclei in 3d systems with solid-liquid[81,82] phases as well as 2d systems with steps at faceted solid-liquid interfaces.[83] In those simulations the total enthalpy in the system was fixed, while in our simulation it was the total number of atoms was fixed. In the case of the non-planar equilibrium the solubility of atoms within each phase at a given temperature is expected to converge to the values of the planar coexistence with increasing size of the nucleus.

Transformations at grain boundaries are not only of fundamental scientific interest, but may also have practical importance by affecting the properties of materials. Experimental studies demonstrated discontinuous changes in properties of polycrystalline materials and bicrystals, linking grain boundary phase transitions to abnormal grain growth, activated sintering and grain boundary embrittlement.[3,6,84–88] Multiple GB phases found by atomistic simulations in fcc Cu provided a convenient model to investigate the importance of GB structure-property relations. Specifically, the simulations revealed that the transitions between these GB structures have a pronounced effect on shear strength and can even reverse the direction of GB migration.[89,90] In a binary Cu(Ag) system, the different GB phases demonstrated distinct monolayer and bi-layer segregation patterns with very different amounts of Ag segregation.[8,20] In other words, the changes in GB structure can dramatically alter the segregation sites and the occupation of these sites by solutes. The detailed investigation of impurity segregation to non-DSC grain boundaries in tungsten and their mechanical properties is the subject of future work.

Our simulations also offer new insights regarding the role of GBs in radiation damage evolution. Nanocrystalline and ultra-fine grain materials have higher radiation tolerance due to increased fraction of GBs that act as sinks and sources for point defects and sites for defects recombination. Several nanometer thick defect free zones are often observed around certain grain boundaries in materials after they were exposed to radiation .[91] However, the role of the boundary character on the sink efficiency and the mechanisms of how the defects interact with GBs

at the nanoscale are not well understood.[92] In our simulations, we show that some high-angle boundaries can absorb point defects through a formation of nanoscale islands of a different GB phase with higher atomic density. These islands may affect mechanical properties of GBs due to stresses generated by GB phase junctions and influence the GB migration. They are also traps for interstitials and may affect the diffusive transport of the interstitials through a polycrystalline network.

In short, in this work we demonstrated new ground states and phase behavior of grain boundaries in a model bcc metal. This rich behavior found in a high-angle and high-energy GBs using the new evolutionary method motivates a systematic investigation of other grain boundaries in bcc metals as well as grain boundary phase transitions in tungsten alloys.

Table I. (top panel) Convergence of grain boundary energy of GB14, E_{GB} (J/m^2), with respect to the number of **k**-points with ENCUT = 250 eV. (bottom panel) Convergence with respect to ENCUT with 2×4×1 **k**-point grid.

k-point grid	2×4×1	3×5×1	3×6×1	4×7×1
E_{GB}	2.680	2.664	2.661	2.670
ENCUT	250 eV	300 eV	350 eV	450 eV
E_{GB}	2.680	2.678	2.680	2.683

ACKNOWLEDGMENT

Label	[n]	EAM1, J/m^2	EAM2, J/m^2	DFT, J/m^2
GB1	1/2	2.819		2.592
GB2	1/2	2.811		2.593
GB3	1/2	2.818		2.594
GB4	1/2	2.807		2.595
GB5	1/2	2.817		2.609
GB6	1/2	2.802		2.610
GB7	1/2	2.798		2.624
GB8	1/2	2.796		2.626
GB9	1/2	2.812		2.628
GB10*	0	3.171		2.960
GB11	1/2		2.493	2.590
GB12	0		2.495	2.951
GB13*	0		2.670	2.973
GB14*	0			2.680

Table II. The grain boundary energy of different structures of the $\Sigma 27(552)[1\bar{1}0]$ symmetric tilt boundary generated with the evolutionary algorithm and the γ-surface approach (*) using the EAM1 and EAM2 potentials and DFT. The second column indicates the atomic density $[n]$ of the different structures as a fraction of the atoms in the (552) plane. Both potentials predict new ground states that were found with the grand-canonical evolutionary search. The ground state is represented by several similar but distinct structures with the same energy within the accuracy of the DFT calculations. GB14 was previously found in Ref.[67].

---

* Current address: Skolkovo Institute of Science and Technology, Skolkovo Innovation Center, 3 Nobel St., Moscow 143026, Russia

[1] A. P. Sutton and R. W. Balluffi, *Interfaces in Crystalline Materials*, Clarendon Press, Oxford, 1995.

[2] M. P. Harmer, Journal of the American Ceramic Society **93**, 301 (2010).

[3] J. Luo, H. Cheng, K. M. Asl, C. J. Kiely, and M. P. Harmer, Science **333**, 1730 (2011).

4   Symbols,   in *Recrystallization and Related Annealing Phenomena (Second Edition)*, edited by F. Humphreys and M. Hatherly, pages xxi – xxii, Elsevier, Oxford, second edition edition, 2004.

5   K. Lu, L. Lu, and S. Suresh, Science **324**, 349 (2009).

6   P. R. Cantwell, M. Tang, S. J. Dillon, J. Luo, G. S. Rohrer, and M. P. Harmer, Acta Materialia **62**, 1 (2014).

7   S. V. Divinski, H. Edelhoff, and S. Prokofjev, Phys. Rev. B **85**, 144104 (2012).

8   T. Frolov, S. V. Divinski, M. Asta, and Y. Mishin, Phys. Rev. Lett. **110**, 255502 (2013).

9   S. J. Dillon and M. P. Harmer, Acta Materialia **55**, 5247 (2007).

10   S. J. Dillon, M. Tang, W. C. Carter, and M. P. Harmer, Acta Mater. **55**, 6208 (2007).

11   S. J. Dillon, K. Tai, and S. Chen, Current Opinion in Solid State and Materials Science **20**, 324 (2016).

12   J. Luo, H. Wang, and Y.-M. Chiang, Journal of the American Ceramic Society **82**, 916 (1999).

13   G. Campbell, J. Belak, and J. Moriarty, Acta Mater. **47**, 3977 (1999).

14   D. Medlin, K. Hattar, J. Zimmerman, F. Abdeljawad, and S. Foiles, Acta Materialia **124**, 383 (2017).

15   K. L. Merkle and D. J. Smith, Phys. Rev. Lett. **59**, 2887 (1987).

16   G. H. Campbell, M. Kumar, W. E. King, J. Belak, J. A. Moriarty, and S. M. Foiles, Philosophical Magazine A **82**, 1573 (2002).

17   T. Frolov, D. L. Olmsted, M. Asta, and Y. Mishin, Nat. Commun. **4**, 1899 (2013).

18   Q. Zhu, A. Samanta, B. Li, R. E. Rudd, and T. Frolov, Nat. Commun. **9**, 467 (2018).

19   T. Frolov, M. Asta, and Y. Mishin, Curr. Opin. Solid State Mater. Sci. **20**, 308 (2016).

20   T. Frolov, M. Asta, and Y. Mishin, Phys. Rev. B **92**, 020103 (2015).

21   K. Morita and H. Nakashima, Materials Science and Engineering: A **234**, 1053 (1997).

22   M. A. Tschopp, K. N. Solanki, F. Gao, X. Sun, M. A. Khaleel, and M. F. Horstemeyer, Phys. Rev. B **85**, 064108 (2012).

23   D. Wolf, Philosophical Magazine Part B **59**, 667 (1989).

24   D. Wolf, Journal of Applied Physics **69**, 185 (1991).

25   D. Yeşilleten and T. A. Arias, Phys. Rev. B **64**, 174101 (2001).

26   S. Ratanaphan, D. L. Olmsted, V. V. Bulatov, E. A. Holm, A. D. Rollett, and G. S. Rohrer, Acta Materialia **88**, 346 (2015).

27   D. L. Olmsted, D. Buta, A. Adland, S. M. Foiles, M. Asta, and A. Karma, Phys. Rev. Lett. **106**, 046101 (2011).

28   S. Zinkle and L. Snead, Annual Review of Materials Research **44**, 241 (2014).

29 D. Maisonnier, D. Campbell, I. Cook, L. D. Pace, L. Giancarli, J. Hayward, A. L. Puma, M. Medrano, P. Norajitra, M. Roccella, P. Sardain, M. Tran, and D. Ward, Nuclear Fusion **47**, 1524 (2007).

30 Y. Mutoh, K. Ichikawa, K. Nagata, and M. Takeuchi, J. of Mat. Sci. **30**, 770 (1995).

31 M. C. Marinica, L. Ventelon, M. R. Gilbert, L. Proville, S. L. Dudarev, J. Marian, G. Bencteux, and F. Willaime, Journal of Physics: Condensed Matter **25**, 395502 (2013).

32 X. Zhou, H. Wadley, R. Johnson, D. Larson, N. Tabat, A. Cerezo, A. Petford-Long, G. Smith, P. Clifton, R. Martens, and T. Kelly, Acta Materialia **49**, 4005 (2001).

33 W. Setyawan and R. J. Kurtz, Journal of Physics: Condensed Matter **26**, 135004 (2014).

34 W. Setyawan and R. J. Kurtz, Scripta Materialia **66**, 558 (2012).

35 S. von Alfthan, P. D. Haynes, K. Kashi, and A. P. Sutton, Phys. Rev. Lett. **96**, 055505 (2006).

36 J. Han, V. Vitek, and D. J. Srolovitz, Acta Mater. **104**, 259 (2016).

37 D. M. Duffy and P. W. Tasker, J. Am. Ceram. Soc **67**, 176 (1984).

38 W. Setyawan and R. J. Kurtz, Scripta Materialia **66**, 558 (2012).

39 X. Wu, Y.-W. You, X.-S. Kong, J.-L. Chen, G. N. Luo, G.-H. Lu, C. S. Liu, and Z. Wang, Acta Materialia **120**, 315 (2016).

40 D. Scheiber, R. Pippan, P. Puschnig, and L. Romaner, Modelling and Simulation in Materials Science and Engineering **24**, 085009 (2016).

41 Z. W. Li, X. S. Kong, Liu-Wei, C. S. Liu, and Q. F. Fang, Chinese Physics B **23**, 106107 (2014).

42 M. K. Miller and A. J. Bryhan, Materials Science and Engineering: A **327**, 80 (2002).

43 T. G. Nieh, Scripta Metallurgica **18**, 1279 (1984).

44 J. R. Rice and J.-S. Wang, Materials Science and Engineering: A **107**, 23 (1989).

45 D. Scheiber, V. I. Razumovskiy, P. Puschnig, R. Pippan, and L. Romaner, Acta Materialia **88**, 180 (2015).

46 P. W. Tasker and D. M. Duffy, Philos. Mag. A **47**, L45 (1983).

47 D. M. Duffy and P. W. Tasker, Philos. Mag. A **53**, 113 (1986).

48 S. R. Phillpot and J. M. Rickman, The Journal of Chemical Physics **97**, 2651 (1992).

49 J. Zhang, C.-Z. Wang, and K.-M. Ho, Phys. Rev. B **80**, 174102 (2009).

50 A. L. S. Chua, N. A. Benedek, L. Chen, M. W. Finnis, and A. P. Sutton, Nat Mater **9**, 418 (2010).

51 W. Yu and M. Demkowicz, Journal of Materials Science **50**, 4047 (2015).

52 I. Novoselov and A. Yanilkin, Computational Materials Science **112, Part A**, 276 (2016).

53 J. Han, V. Vitek, and D. J. Srolovitz, Acta Materialia **133**, 186 (2017).

54 A. M. Reilly et al., Acta Crystallographica Section B **72**, 439 (2016).

55 A. R. Oganov and C. W. Glass, The Journal of Chemical Physics **124**, 244704 (2006).

[56] X.-F. Zhou, X. Dong, A. R. Oganov, Q. Zhu, Y. Tian, and H.-T. Wang, Phys. Rev. Lett. **112**, 085502 (2014).

[57] Q. Zhu, L. Li, A. R. Oganov, and P. B. Allen, Phys. Rev. B **87**, 195317 (2013).

[58] Q. Zhu, V. Sharma, A. R. Oganov, and R. Ramprasad, The Journal of Chemical Physics **141**, 154102 (2014).

[59] A. O. Lyakhov, A. R. Oganov, H. T. Stokes, and Q. Zhu, Computer Physics Communications **184**, 1172 (2013).

[60] A. R. Oganov, A. O. Lyakhov, and M. Valle, Accounts of Chemical Research **44**, 227 (2011).

[61] Q. Zhu, A. R. Oganov, A. O. Lyakhov, and X. Yu, Phys. Rev. B **92**, 024106 (2015).

[62] S. Plimpton, J. Comput. Phys. **117**, 1 (1995).

[63] A. O. Lyakhov, A. R. Oganov, and M. Valle, Comput. Phys. Commun. **181**, 1623 (2010).

[64] G. Kresse and J. Furthmuller, Physical Review B **54**, 11169 (1996).

[65] G. Kresse and D. Joubert, Physical Review B **59**, 1758 (1999).

[66] J. P. Perdew, K. Burke, and M. Ernzerhof, Physical Review Letters **77**, 3865 (1996).

[67] W. Setyawan and R. J. Kurtz, Journal of Physics: Condensed Matter **26**, 135004 (2014).

[68] G. P. Pun, K. Darling, L. Kecskes, and Y. Mishin, Acta Materialia **100**, 377 (2015).

[69] X. W. Zhou, R. A. Johnson, and H. N. G. Wadley, Phys. Rev. B **69**, 144113 (2004).

[70] R. G. Hoagland and R. J. Kurtz, Philos. Mag. A **82**, 1073 (2002).

[71] F. Lançon, T. Radetic, and U. Dahmen, Phys. Rev. B **69**, 172102 (2004).

[72] T. Radetic, F. Lançon, and U. Dahmen, Phys. Rev. Lett. **89**, 085502 (2002).

[73] A. Stukowski, Modell. Simul. Mater. Sci. Eng. **18**, 015012 (2010).

[74] T. Frolov and Y. Mishin, J. Chem. Phys. **143**, 044706 (2015).

[75] J. W. Gibbs, *The Scientific Papers of J. Willard Gibbs*, volume 1, Longmans-Green, London, 1906.

[76] F. C. Larche and J. W. Cahn, Acta Metall. **26**, 1579 (1978).

[77] W. W. Mullins and R. F. Sekerka, The Journal of Chemical Physics **82**, 5192 (1985).

[78] P. Voorhees and W. C. Johnson, The thermodynamics of elastically stressed crystals, volume 59 of *Solid State Physics*, pages 1 – 201, Academic Press, 2004.

[79] T. Frolov and Y. Mishin, Phys. Rev. B **85**, 224106 (2012).

[80] T. Frolov and Y. Mishin, Phys. Rev. B **85**, 224107 (2012).

[81] T. Frolov and Y. Mishin, Phys. Rev. Lett. **106**, 155702 (2011).

[82] L. A. Zepeda-Ruiz, B. Sadigh, A. A. Chernov, T. Haxhimali, A. Samanta, T. Oppelstrup, S. Hamel, L. X. Benedict, and J. L. Belof, The Journal of Chemical Physics **147**, 194704 (2017).

[83] T. Frolov and M. Asta, The Journal of Chemical Physics **137**, 214108 (2012).
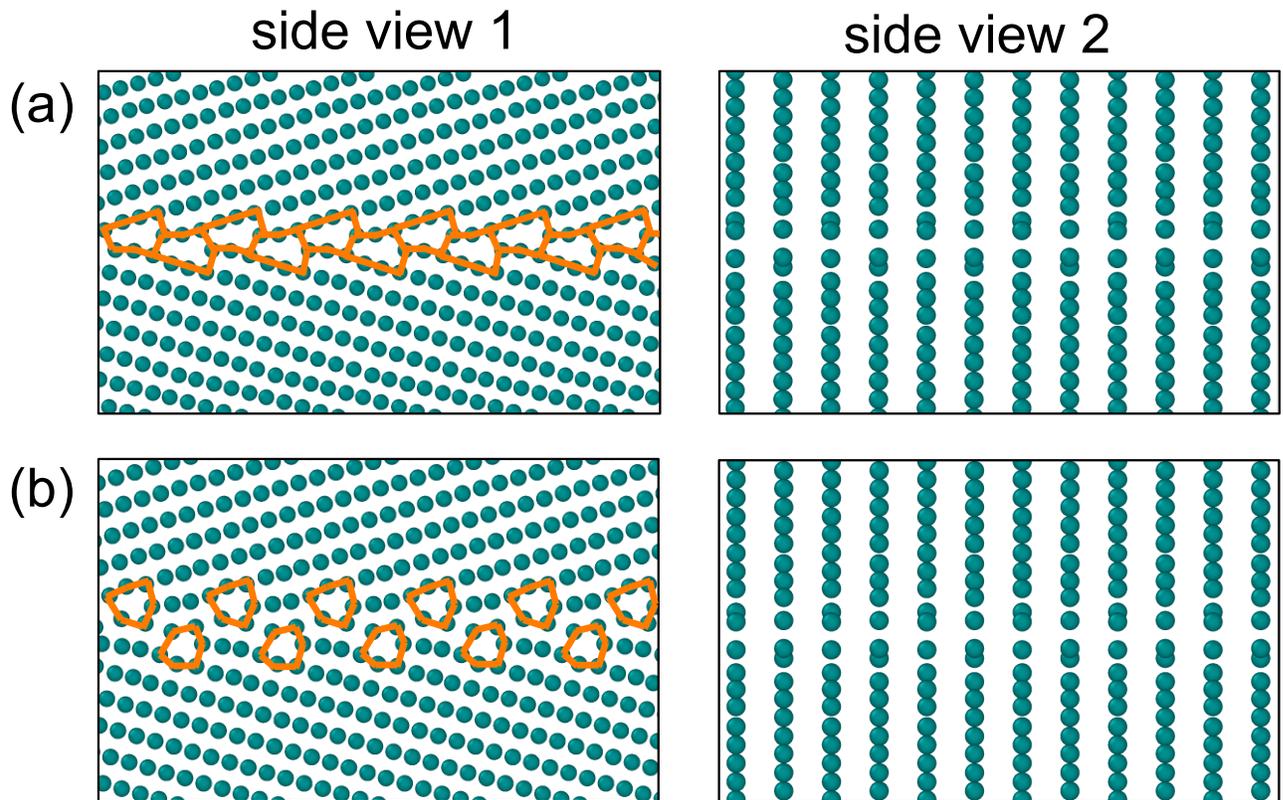
Figure 1. γ-surface constructed $\Sigma27(552)[1\bar{1}0]$ GB in W using (a) DFT[67] and (b) the EAM1[32] and EAM2[31] potentials.

[84]   M. Baram, D. Chatain, and W. D. Kaplan, Science **332**, 206 (2011).

[85]   M. P. Harmer, Science **332**, 182 (2011).

[86]   W. Rheinheimer and M. J. Hoffmann, Scripta Materialia **101**, 68 (2015).

[87]   J. D. Schuler and T. J. Rupert, Acta Materialia **140**, 196 (2017).

[88]   G. S. Rohrer, Curr. Opin. Solid State Mater. Sci. **20**, 231 (2016).

[89]   T. Frolov, Appl. Phys. Lett. **104**, 211905 (2014).

[90]   V. Borovikov, X.-Z. Tang, D. Perez, X.M. Bai, B. P. Uberuaga, and A. F. Voter, Journal of Physics: Condensed Matter **25**, 035402 (2013).

[91]   W. Han, M. Demkowicz, E. Fu, Y. Wang, and A. Misra, Acta Materialia **60**, 6341 (2012).

[92]   X.M. Bai, A. F. Voter, R. G. Hoagland, M. Nastasi, and B. P. Uberuaga, Science **327**, 1631 (2010).
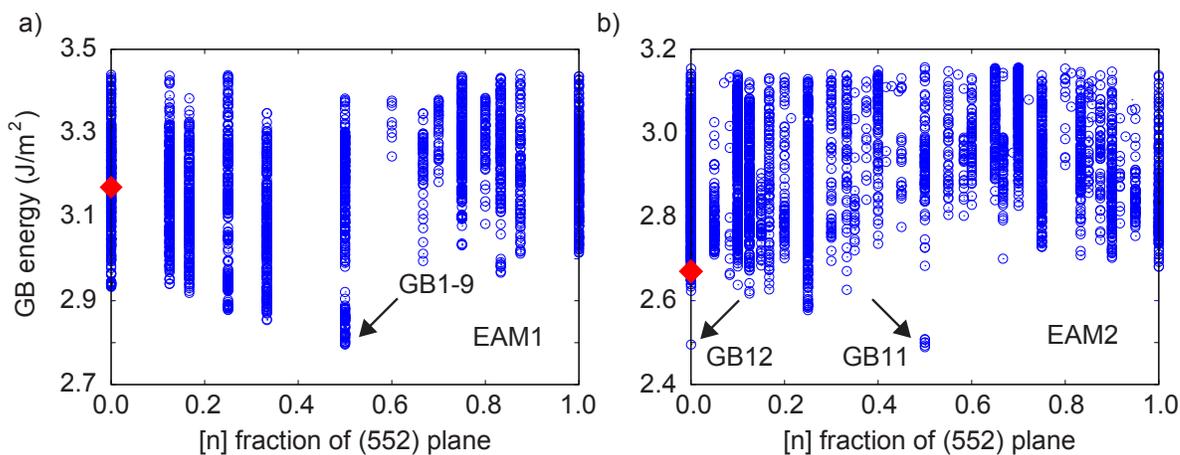
Figure 2. Results of the evolutionary search. The grain boundary energy for different structures of the $\Sigma27(552)[1\bar{1}0]$ boundary in W generated by the evolutionary search with (a) the EAM1[31] and (b) EAM2[32] potentials. The energy is plotted as a function of the number of atoms [n] expressed as a fraction of atoms in the (552) plane. The red diamonds on the plots represent the best configurations generated by the conventional γ-surface approach. The arrows point to new ground states with different atomic densities predicted by the evolutionary search.
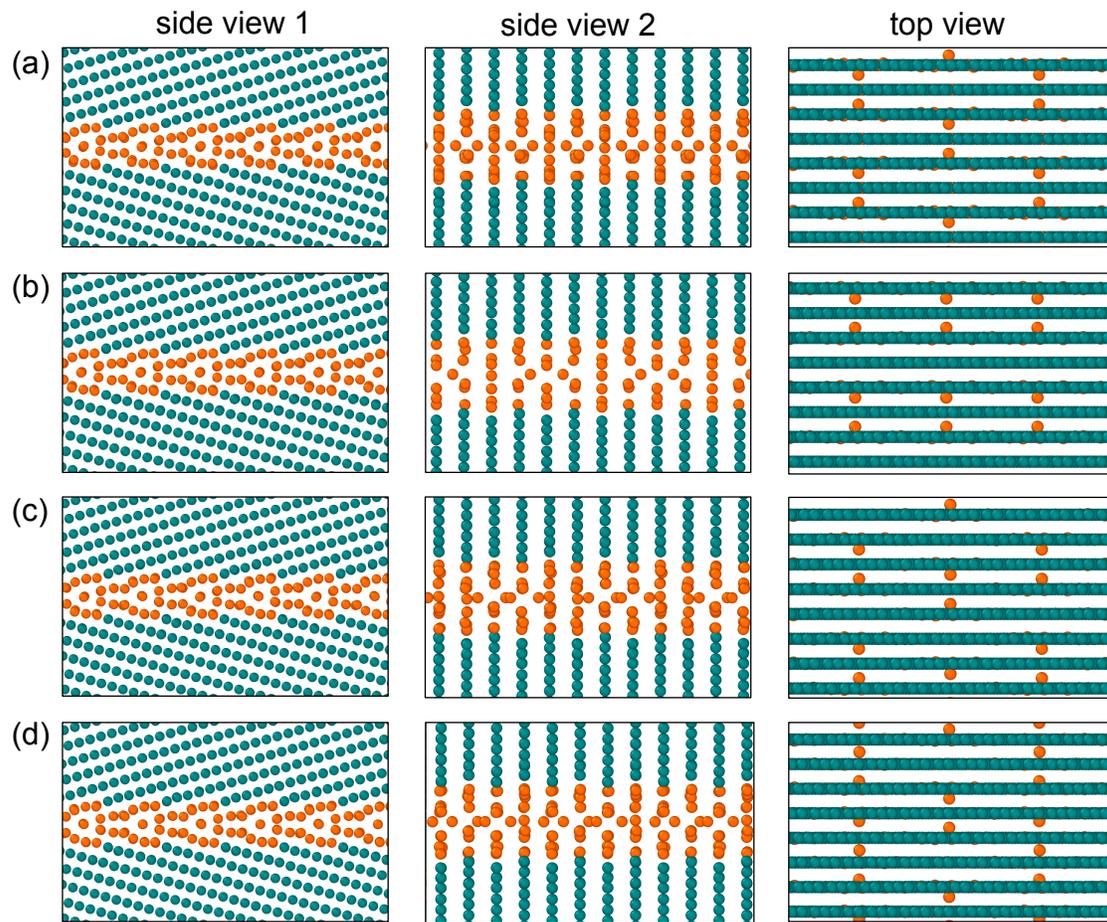
Figure 3. New [n]=1/2 ground state structures of the $\Sigma27(552)[1\bar{1}0]$ GB in W predicted by the evolutionary structure search with the EAM1[31] and EAM2[32] potentials: (a) GB11, (b) GB1, (c) GB2 and (d) GB3. The DFT calculations confirm these to be the lowest energy states with the energies $\gamma_{\text{GB}} = 2.59$ J/m^2 identical within the accuracy of the calculations. Bulk (green) and grain boundary (orange) atoms are colored according to the common neighbor analysis[73].
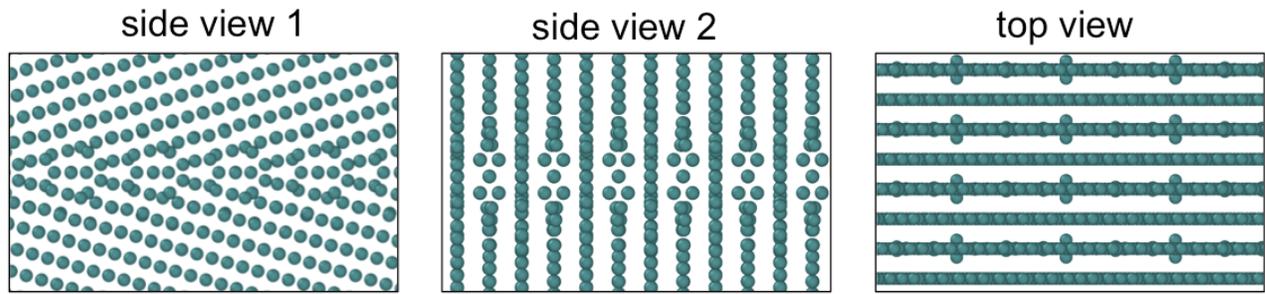
Figure 4. GB12 structure of the $\Sigma27(552)[1\bar{1}0]$ GB in W predicted by the evolutionary search at $[n]_{\text{GB12}} = 0$ with the EAM2 potential[32]. The energy of this structure $\gamma_{\text{GB12}} = 2.495$ J/m^2 is identical within the accuracy of the calculations to the energy of the ground state structure GB11 with $\gamma_{\text{GB11}} = 2.493$ J/m^2 and $[n]_{\text{GB11}} = 1/2$ (cf. Fig. 3a). This structure has the same number of atoms as the γ-surface structure, but the energy is 7% lower. In this case no atoms were inserted or removed from the GB core, however the evolutionary search finds this low-energy structure by rearranging the GB atoms.
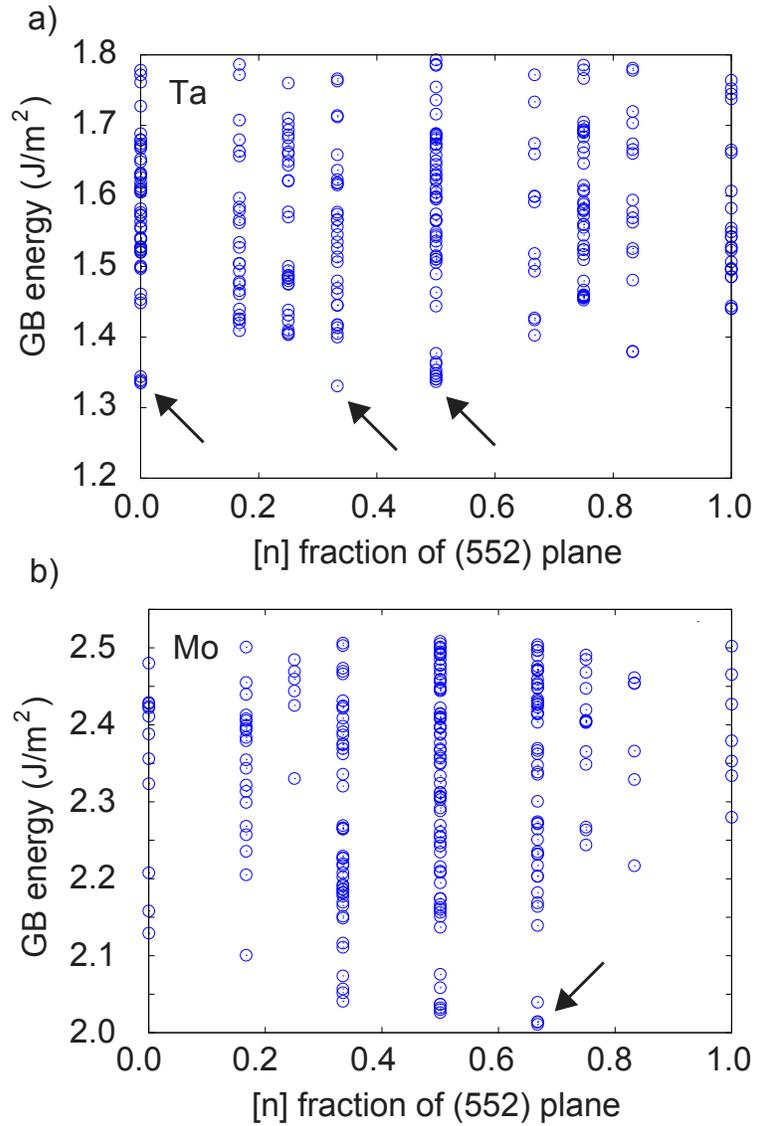
Figure 5. Results of the evolutionary search. The grain boundary energy for different structures of the $\Sigma27(552)[1\bar{1}0]$ boundary in Ta and Mo. The energy is plotted as a function of the number of atoms [n] expressed as a fraction of atoms in the (552) plane. The arrows point to new ground states with different atomic densities predicted by the evolutionary search.
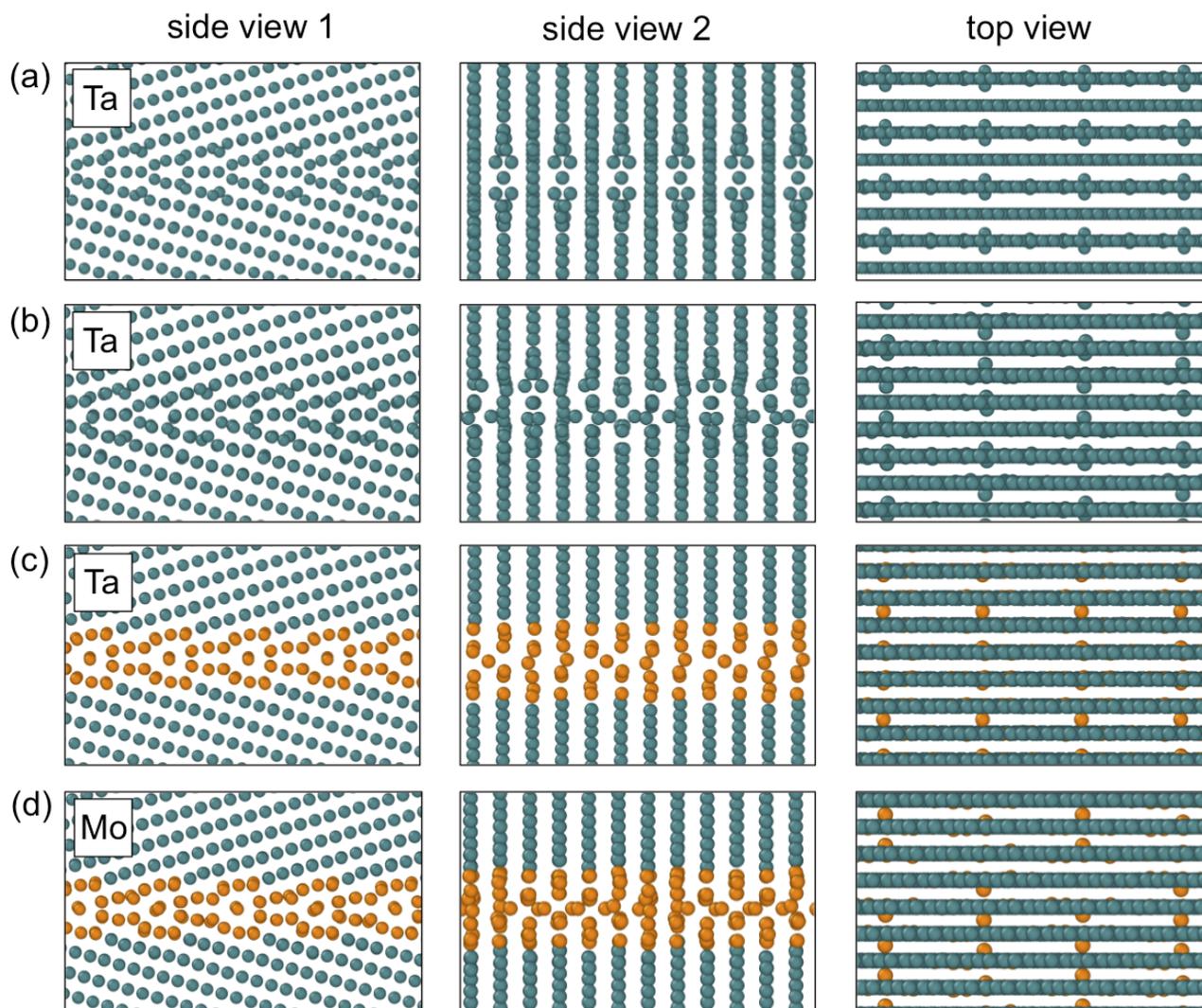
Figure 6. New ground states and low-energy structures of the $\Sigma27(552)[1\bar{1}0]$ GB in Ta and Mo. The Ta search identified a) [n]=0 GB structure that was also predicted by EAM2 potential in W, b) a ground state at [n]=1/3, which is a denser version of a). GB structures c) with [n]=1/2 and d) with [n]=2/3 are variations of the [n]=1/2 ground state found in W. a) is a 2×2 GB area reconstruction, while b), c) and d) are 2×3 reconstructions.
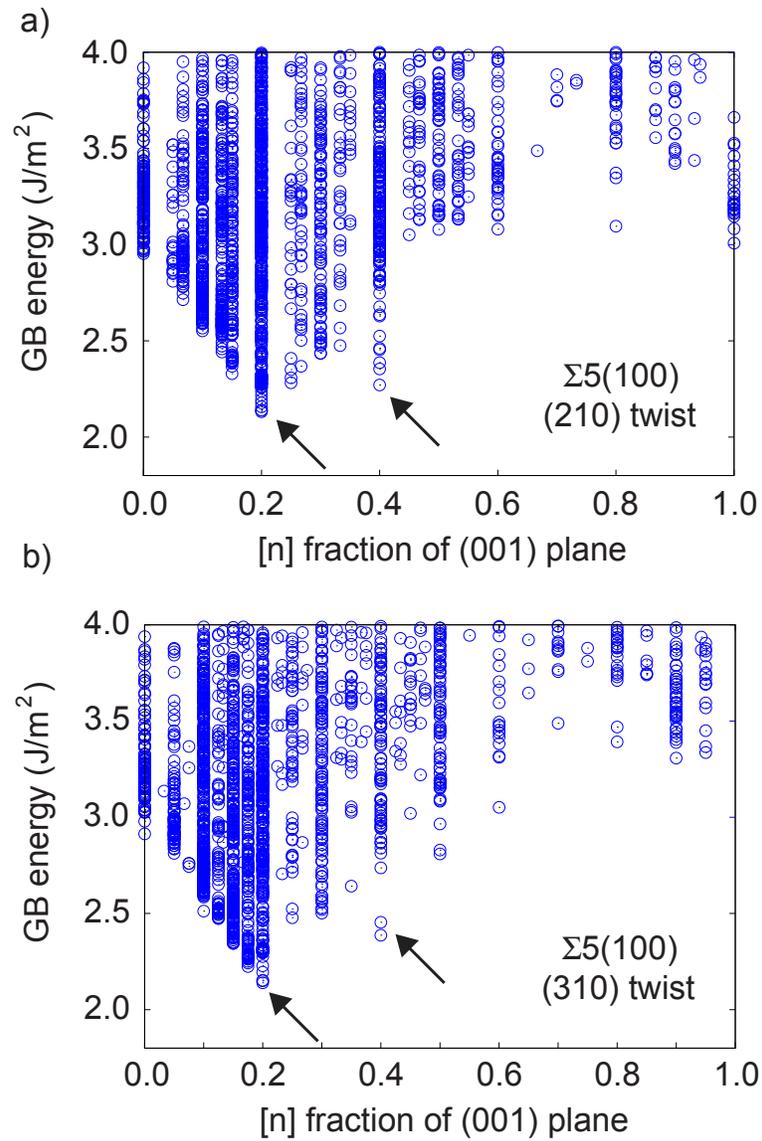
Figure 7. Results of the evolutionary search for the $\Sigma5(001)$ twist boundaries. The energy is plotted as a function of the number of atoms [n] expressed as a fraction of atoms in the (001) plane. The arrows point to ground states at [n]=1/5 and metastable states at [n]=2/5. These states are examples of different GB phases.
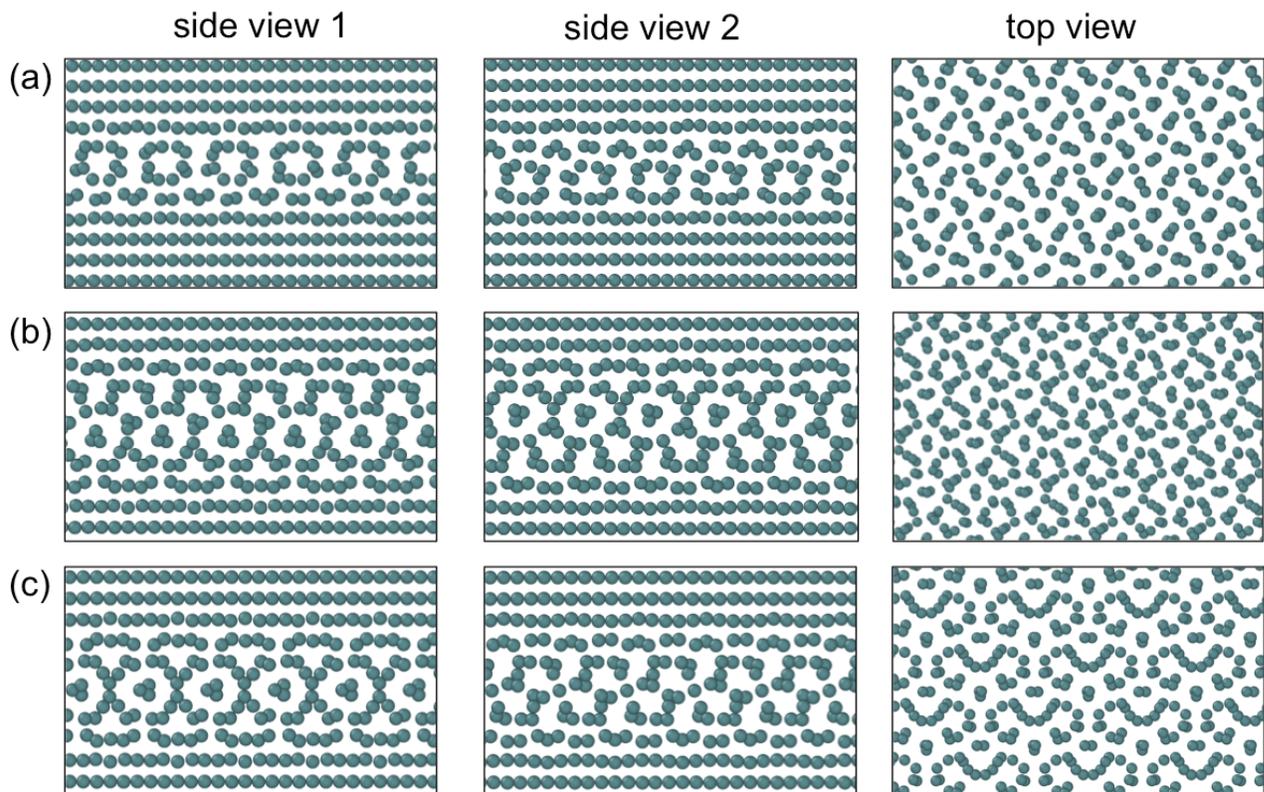
Figure 8. Grain boundary phases of the $\Sigma5(001)$ (310)-twist boundary $\theta = 36.87°$ in W predicted by the evolutionary search with EAM2 potential. a) Ground state at 0K with [n]=1/5 and energy $\gamma_{GB} = 2.28$ J/m^2. b) and c) are examples of [n]=2/5 states with different symmetries and energies $\gamma_{GB} = 2.49$ J/m^2 and $\gamma_{GB} = 2.38$ J/m^2, respectively. GB structures in a) and b) left-hand side and middle panels are horizontal mirror images of each other. GB structure in c) on the other hand is not, while it has the lowest energy at [n]=2/5.

side view 1

side view 2

top view
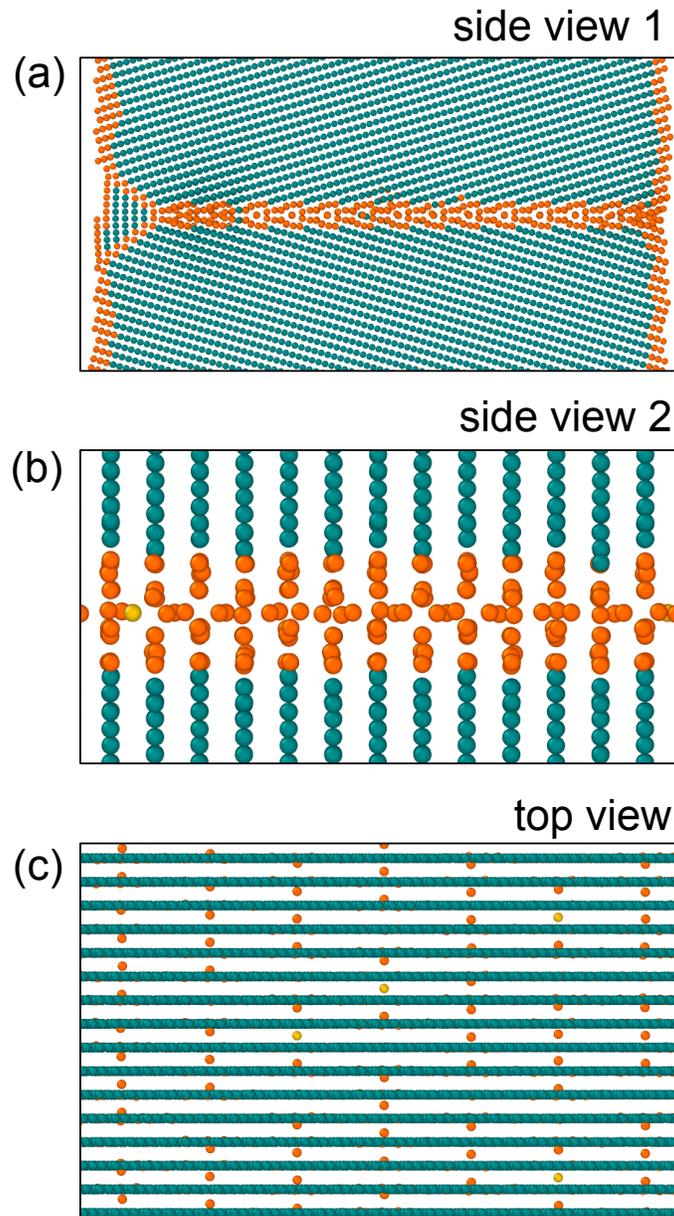
Figure 9. Equilibrium structure of the $\Sigma27(552)[1\bar{1}0]$ GB at T=2500 K modeled with the EAM1 potential. A 100 ns long isothermal molecular dynamic simulation with the GB terminated at two open surfaces predicts the high-temperature GB structure independently from the 0 K search. Bulk (green) and grain boundary (orange) atoms are colored according to the common neighbor analysis.[73]
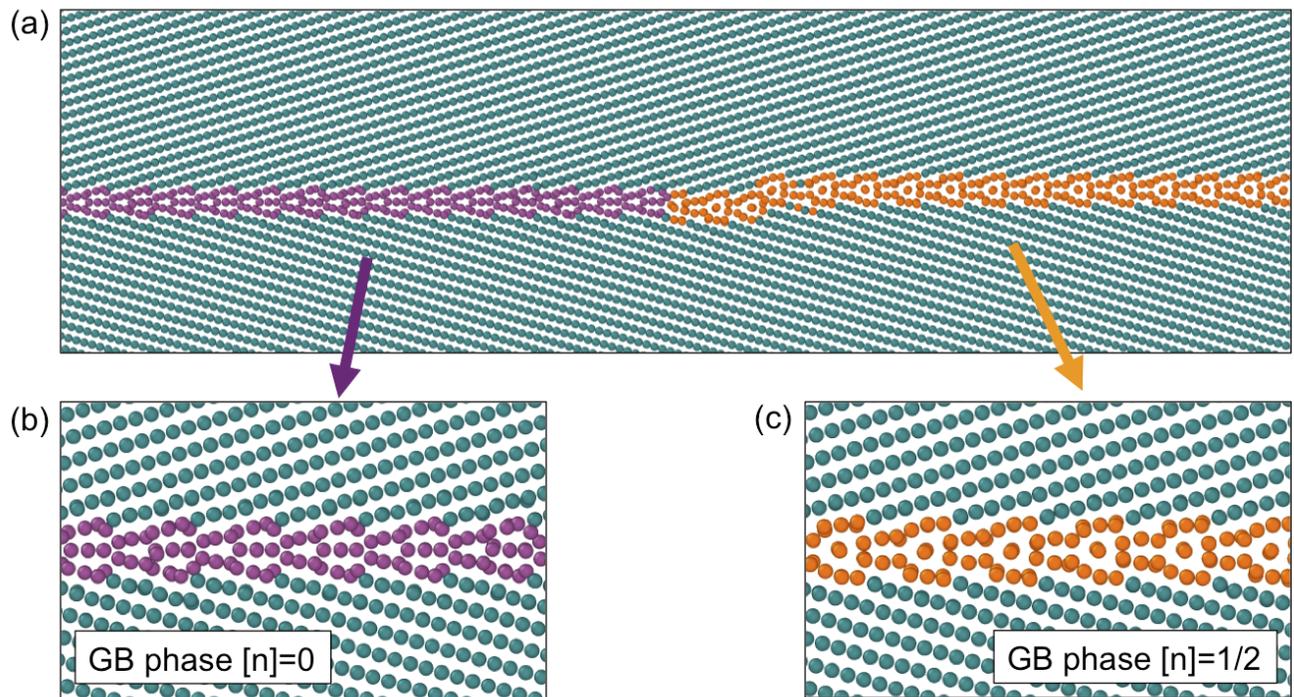
Figure 10. (a) Two grain boundary phases [n]=0 and [n]=1/2 in W coexisting in equilibrium at T=2000 K for 200 ns in a closed system with periodic boundary conditions along the boundary. b) and c) show closer views of the two structures. The equilibrium is established through the exchange of atoms between the two GB phases. The coexistence simulation demonstrates that the two types of structures predicted by the evolutionary search at 0 K represent two different GB phases. The γ-surface approach fails to predict both of these finite-temperature structures. In the figure the bulk (green) and the grain boundary (orange, magenta) atoms are colored according to the common neighbor analysis.[73]
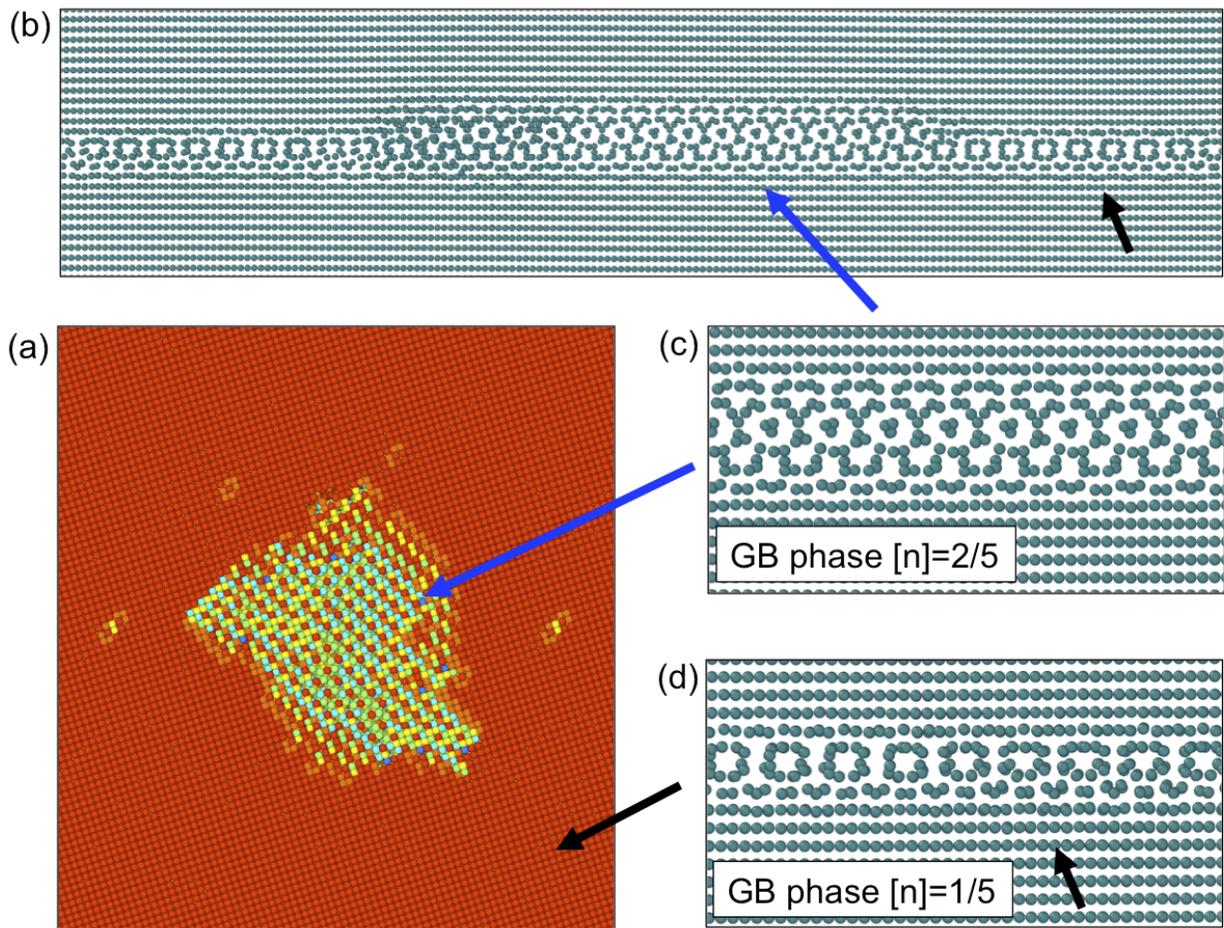
Figure 11. (a) Nanoscale nucleus of the [n]=2/5 GB phase inside the parent [n]=1/5 GB phase of the $\Sigma5(001)$ (310)-twist boundary in W which appeared as a result of the absorption of interstitial atoms. (b) Cut through the nucleus shows the heterogeneous structure of the GB. c) and d) show closer views of the two structures. The two GB phases [n]=2/5 and [n]=1/5 coexist in equilibrium at T=3000 K in a closed system with periodic boundary conditions along the boundary. The two GB phases are separated by curved or non-planar GB phase junction. The equilibrium is established through the exchange of atoms between the two GB phases. The coexistence simulation demonstrates that the two types of structures predicted by the evolutionary search at 0 K represent two different GB phases.[73]